Purified Graphene Oxide Dispersions Lack In Vitro Cytotoxicity and In Vivo Pathogenicity

*Hanene Ali-Boucetta, Dimitrios Bitounis, Rahul Raveendran-Nair, Ania Servant, Jeroen Van den Bossche, and Kostas Kostarelos**

Prompted by the excitement from the description of single layer graphene, increased attention for potential applications in the biomedical field has been recently placed on graphene oxide (GO). Determination of the opportunities and limitations that GO offers in biomedicine are particularly prone to inaccuracies due to wide variability in the preparation methodologies of GO material in different laboratories, that results in significant variation in the purity of the material and the yield of the oxidation reactions, primarily the Hummers method used. Herein, the fabrication of highly pure, colloidally stable, and evenly dispersed GO in physiologically-relevant aqueous buffers in comparison to conventional GO is investigated. The purified GO material is thoroughly characterized by a battery of techniques, and is shown to consist of single layer GO sheets of lateral dimensions below 500 nm. The cytotoxic impact of the GO in vitro and its inflammation profile in vivo is investigated. The purified GO prepared and characterized here does not induce significant cytotoxic responses in vitro, or inflammation and granuloma formation in vivo following intraperitoneal injection. This is one of the initial steps towards determination of the safety risks associated with GO material that may be interacting with living tissue.

1. Introduction

Graphene is a two-dimensional material with unique physicochemical properties (including electrical, thermal and optical) that holds great promise for advanced material science, electronics and energy applications.[1–4] During the last few years graphene-based materials have also been attracting tremendous attention in the biomedical field. In particular, graphene oxide sheets (GO),[5] are becoming some of the most important graphene derivatives investigated for biomedical applications,[6,7] ranging from biosensors,[8–10] to drug delivery vectors.[11–13]

Today, mainly proof-of-concept studies with GO have investigated their ability to transport therapeutic and diagnostic agents within cells[11] and whole-body imaging[14,15] mainly for the development of anticancer therapeutics.[11,16–18] Their use in photothermal therapy of tumors has also been reported, due to their strong optical properties and absorbance at the near infrared region.[13,19] In addition, some initial cytotoxicity and toxicological studies to determine any possible limitations from use of GO and its overall biocompatibility have been conducted,[20–28] providing yet inconclusive evidence, primarily due to great variability among the graphene material and the assays studied.

One of the key parameters in the development of any nanomaterial for biomedical applications is the control and reproducibility of the structural, surface and colloidal properties of its aqueous dispersion.[29,30] In the case of GO, the most popular methodology employed for its synthesis is currently the chemical oxidation of graphite following either the Brodie, Staudenmaier,[5] or the Hummers[31] protocols. The latter is perhaps the most used method for the preparation of GO and involves the use of strong acids and highly oxidizing reagents that form oxygenated graphene sheets. However, the yield from the Hummers reaction is heterogeneous and contains a large fraction of unreacted graphite. In addition, the aqueous dispersibility of the end-product is not stable over time. Poor control of the quality and purity of the GO dispersions can retract their successful development for biomedical applications. For instance, variation in the purity of the starting material, the conditions of oxidation and the reagents used, can yield GO samples of different oxidation degrees, dispersibility and impurities.[32] Previously reported studies conducted with GO samples that were prepared in different ways and contained various derivatives, ranged from reduced GO to GO coated or grafted with polyethylene glycol,[11] to amine-modified GO.[33] This means that comparisons as well

Dr. H. Ali-Boucetta,[+] D. Bitounis,[+] Dr. A. Servant, Dr. J. Van den Bossche, Prof. K. Kostarelos
Nanomedicine Laboratory
Centre for Drug Delivery Research
UCL School of Pharmacy
University College London
Brunswick Square
London, WC1N 1AX, UK
E-mail: k.kostarelos@ucl.ac.uk
Dr. R. Raveendran-Nair
School of Physics and Astronomy and Manchester
Centre for Mesoscience & Nanotechnology
University of Manchester
Manchester M13 9PL, UK
[+]These authors contributed equally to this work.

DOI: 10.1002/adhm.201200248

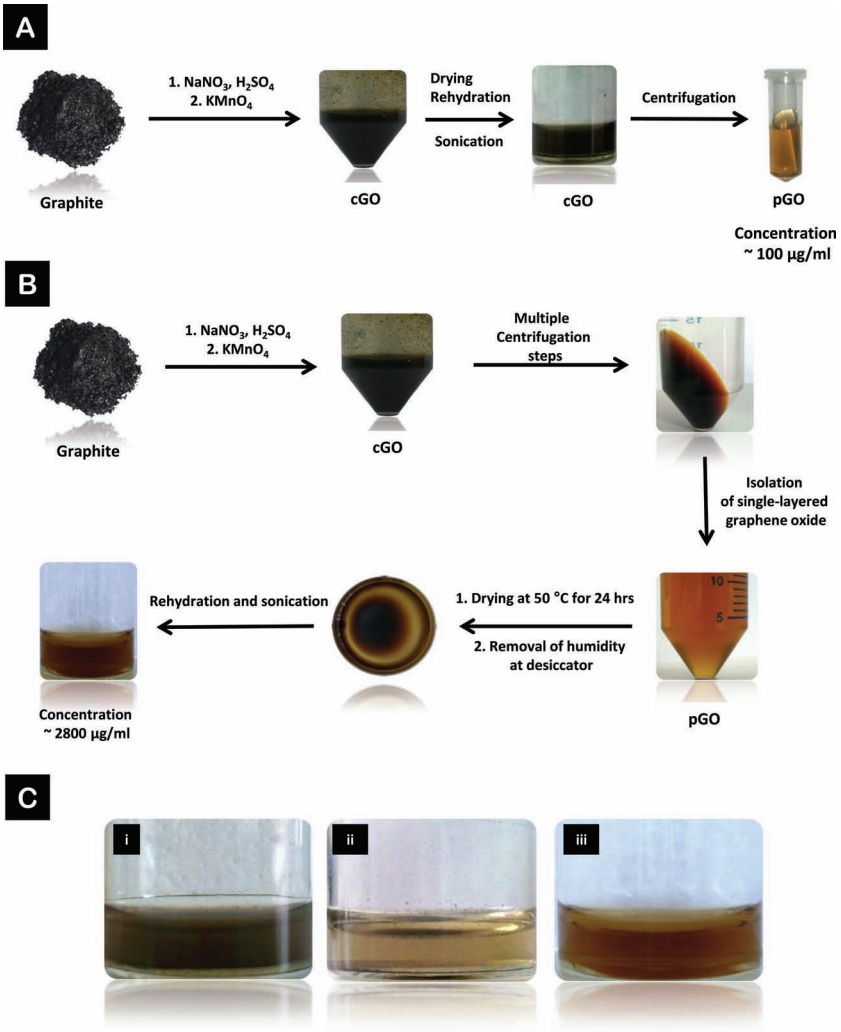

Figure 1. A) Schematic representation of the preparation of graphene oxide (cGO) dispersion by the conventional methodology; B) Schematic representation of the preparation of graphene oxide (pGO) dispersions by the purified process; C) Macroscopic examination of the different GO dispersion: (i) Graphene oxide dispersion prepared by the conventional method few minutes after sonication, (ii) conventional GO 24 h post-dispersion, and (iii) GO dispersion prepared by the purified method.

as generalisations about the opportunities and limitations of GO in biomedicine are particularly prone to inaccuracies. In this study, we attempted the preparation of high-purity, high aqueous dispersibility GO that is colloidally stable and can be easily modified and used for biological investigations more reliably.

2. Results & Discussion

2.1. Preparation of GO Aqueous Dispersions

For the preparation of conventional graphene oxide (cGO) dispersions the method described by Hummers and Offeman,[31] was followed, however, since the oxidation reaction of graphite commonly yields a mixture of graphite oxide and unreacted graphitic fractions (cGO, **Figure 1**A), we have adapted the method by further purification and centrifugation steps[34] to allow the isolation of the purest fraction of GO in the absence of by-products or contaminants.

Others have previously tried to isolate the pure fraction of GO by centrifugation of the final product, however this did not produce high yields of pGO. The maximum concentration we achieved using this methodology was around 100 µg/ml as determined by UV-Vis analysis from a calibration curve of the final product (cGO) of the Hummers method. Even though this is currently the most common methodology to determine GO concentration, we consider it to be unreliable since the colloidal stability of cGO is not acceptable and can easily lead to variation. We attempted to improve the overall methodology by introducing several washing and centrifugation steps until the pH of the cGO dispersion reached 7. As the pH of the cGO dispersion increased, a gel–like brown layer of pure GO appeared at the top of the sample until the pH became neutral (Figure 1B). Although this effect was initially reported by Rourke et al.[34] no further emphasis has since been placed by others, in particular those exploring the material in biology. To accurately determine the concentration of purified GO (pGO) the sample was dried overnight in vacuum at 40 °C. Interestingly, we achieved a concentration of ca.3 mg/ml which is 25-fold higher than the yield achieved by the simple centrifugation protocols of cGO used by most other laboratories (Figure 1A&B). The resuspension of the dried pGO sample took place almost readily in aqueous media, further indicating the enhanced solubility of the material achieved.

2.2. Structural and Colloidal Characterization of the GO Dispersions

The modified protocol for the fabrication of high-purity GO sheets exhibited aqueous dispersibility and colloidal stability over time. Figure 1C shows the colloidal stability of pGO compared to conventional cGO (sediment precipitated and was observed after 24 h at room temperature). We then characterised the size and thickness of the different GO sheets from the aqueously dispersed samples using transmission electron (TEM) and atomic force microscopy (AFM).

As can be observed from **Figure 2**A, the GO sheets produced by the conventional methodology (cGO) were large and formed by lateral stacking of multiple sheets, as could be determined from the contrast of the graphene sheets deposited on the TEM grid. On the other hand, by the optimised methodology developed here significantly smaller and thinner pGO sheets were yielded (Figure 2C). Further analysis of the TEM data (by use

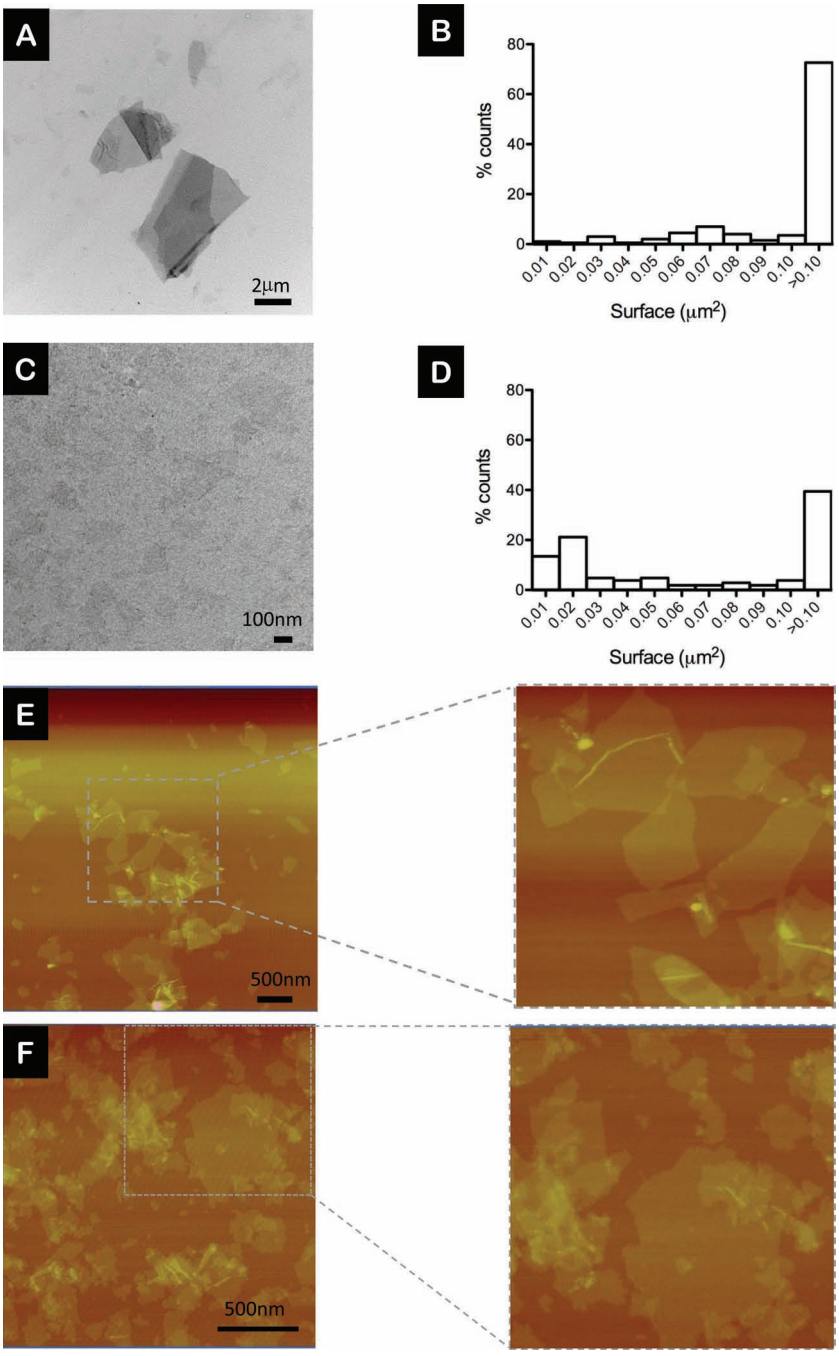

Figure 2. TEM images of graphene oxide (GO) dispersion prepared by the conventional (A) and purified method (C). Size distribution histograms of conventional GO (B) and purified GO (D). E,F) AFM images show the surface and the thickness of the conventional GO (E) and purified GO (F) dispersion. Dashed squares show zoomed-in areas of (E) and (F).

of Image J software for ~ 70–80 sheets/sample) revealed a shift in the distribution of GO sheet dimensions (in μm^2) to smaller values between the conventional and purified GO. Most of the sheets in cGO were larger than 0.10 μm^2 (Figure 2B), while in the case of pGO a significantly smaller distribution of sizes (0.01–0.02 μm^2) was observed (Figure 2D). Furthermore, the thickness of the purified GO sheets was measured ca.1 nm by AFM (Figure 2E&F and Supporting Information (SI), Figure S1). This was thought to correspond to single layer GO as previously reported by others.[35,36]

2.3. Spectroscopic Characterization of the GO Dispersions

In order to monitor the degree of oxidation of the GO sheets following the different protocols, Fourier-transform infrared (FTIR) and ultraviolet-visible (UV-Vis) spectroscopy were performed. **Figure 3**A shows a similar FTIR spectrum for cGO and pGO which suggests that a significant fraction of the graphitic material was successfully oxidised.

The chemical groups (mainly carbonyls, hydroxyls and epoxides) detected were also almost identical for both cGO and pGO. In addition a comparison of the UV-vis spectra of the cGO and pGO dispersions (Figure 3B) indicated a sharper absorption peak around 230nm for the pGO, that is thought to be due to the transition of π to π^* of the C = C bonds and is consistent with what is also described in the literature for GO.[37,38] The intensity of the absorption spectrum for cGO was lower than that of the pGO which further suggested less sites of oxidation in the case of cGO in comparison to pGO. Moreover, we further confirmed the presence of GO in both the cGO and pGO samples using Raman spectroscopy. Figure 3C supports the existence of GO sheets evidenced by the presence of a broad G band (~1590 cm^{-1}) and the appearance of a D band (~1350 cm^{-1}), a consequence of sp^3 domains due to oxidation of graphite.

2.4. Internalisation and Cytotoxicity of GO Dispersions

We then investigated the cellular interaction of the two types of GO suspensions using the human A549 lung carcinoma cell line at different material exposure doses ranging from 7.8 to 125 μg/ml. As observed in **Figure 4**A, incubation with the cGO sample showed large, black aggregate deposits interacting with cells, while pGO could hardly be visible with the optical microscope (Figure 4A, bottom panel). This was explained by the presence of unreacted graphite and graphite oxide aggregates in the cGO dispersions and further indicated that GO samples prepared in this way contain significant amounts of impurities. The pGO dispersions were difficult to visualise because they consisted predominantly of smaller, single layer GO sheets.

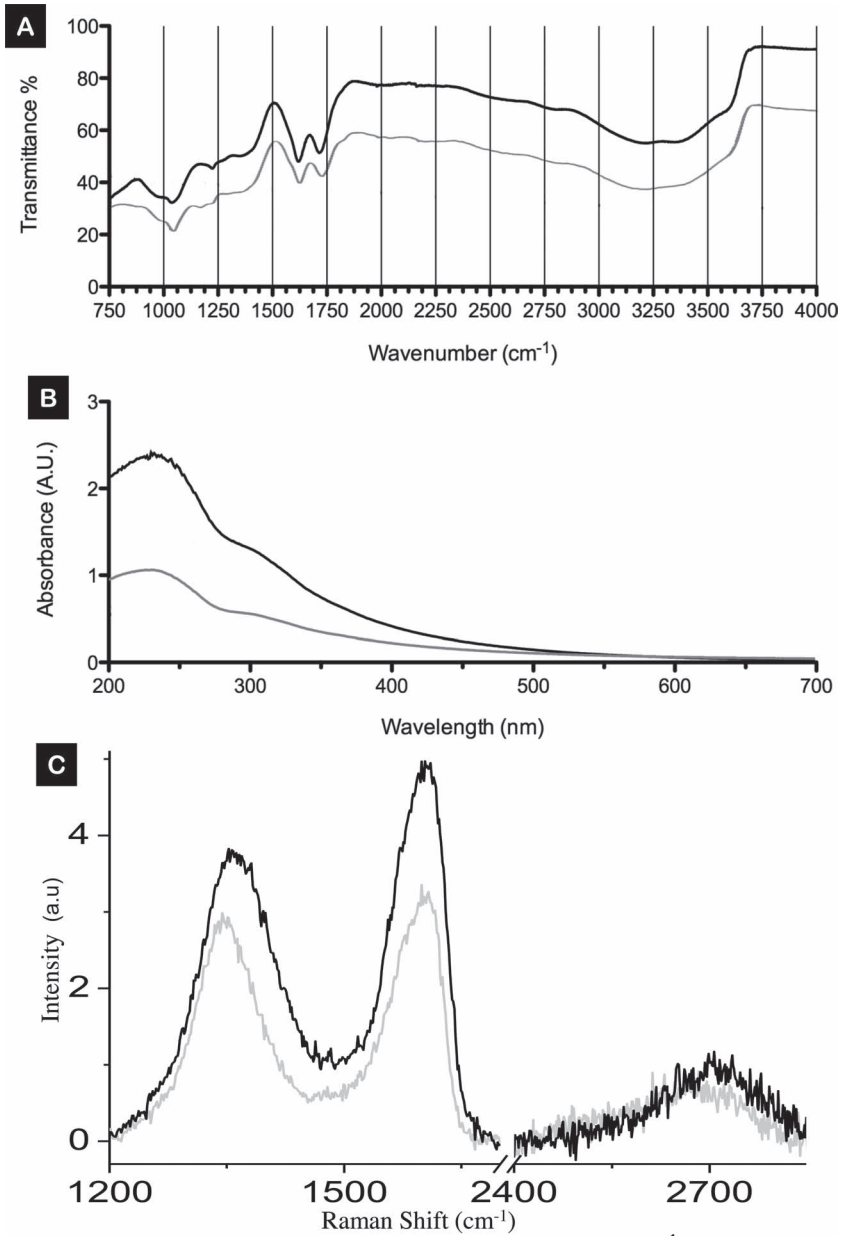

Figure 3. Spectroscopy evaluation of graphene oxide (GO) dispersion prepared by the conventional (grey line) and purified method (black line), as shown by FTIR (A), UV-Vis (B), and Raman (C) spectroscopy techniques. The smooth background due to luminescence of GO in the Raman spectrum was removed.

two GO types. The cGO dispersions despite containing a mixture of graphitic material, they showed only 80% cell viability at the highest dose of exposure. This was very similar to our previously published observations using chemically functionalised carbon nanotubes at the same dose and cell type, and may be due to the poor dispersibility of the material that reduces the effective dose interacting with the cells.[39] Although comparisons should be drawn cautiously, Chang et al.[20] reported that GO (prepared by a different modification of the Hummers method that involved a second reaction cycle followed by filtration and centrifugation) was not uptaken by A549 cells and showed no signs of cytotoxicity, however dose-dependent oxidative stress were obtained. It was speculated that this would be dependent on GO dose and dimensions, but no further evidence for such mechanisms was offered. In contrast, Hu et al.[25] used a similar method to that of Chang et al. for the preparation of GO dispersions, and described dose-dependent cytotoxicity from GO exposure on A549 cells. However, in the latter study the MTT assay that was used to assess cytotoxic responses[25] has been repeatedly shown to be unreliable in the presence of carbon nanomaterials.[39–41] The GO dispersions in Hu et al. were also incubated in serum-containing media, and the effect of serum proteins in the media was speculated as a contributing factor towards GO-mediated cytotoxicity. More recently, another study[42] investigated two methodologies for the successful stabilisation of GO in electrolyte solutions, either via the Hummers method or through dispersion of GO using a tri-block copolymer (Pluronic F127). Their cellular uptake in cervical cancer cells (HeLa) enhanced cytotoxicity for the copolymer-coated GO, similar to what some of us have also previously reported[39] for F127-coated carbon nanotubes. Overall, at this early phase in the development and investigation of graphene material on interaction with living matter, and due to the variation in the graphene oxide preparation protocols, the purification processes and cytotoxicity assays used, one should be extremely careful in drawing generalised conclusions about any possible adverse effect of GO on cell cultures.

In order to further interrogate the possible adverse effects on cell viability following interaction with the GO material, we studied the cytotoxic responses of the cGO and pGO dispersions using the '*modified*'' LDH assay. This is a modified version of a commonly used cytotoxicity assay that we previously developed and reported in order to reliably assess the viability of cell cultures after exposure to carbon nanomaterials devoid of any unwanted interference.[39] As shown in Figure 4B, there was a statistically significant dose-dependent cytotoxic response from exposure to both cGO and pGO compared to untreated cells, however without any significant differences between the

2.5. In Vivo Toxicological Profile of the pGO

To further determine the toxicological adverse responses from exposure to the GO material prepared in this study, we studied the acute and chronic inflammatory response at the peritoneal mesothelial membrane following peritoneal cavity exposure

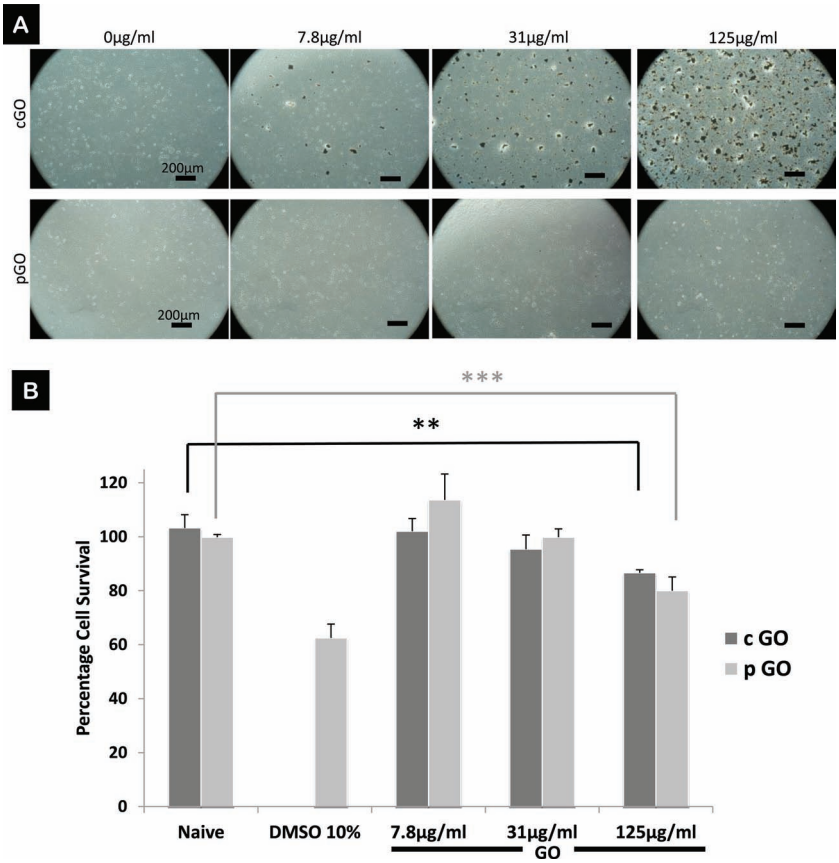

Figure 4. A) Cellular interaction of the conventional (c) and purified (p) GO with A549 cells at different concentrations (7.8–125 µg/mL) for 24 h. The conventional GO (cGO) shows large black aggregates which could be a mixture of graphite and graphite oxide. Lens magnification is ×10. B) Cytotoxicity assessment of A549 cells after treatment with of the conventional (c) and purified (p) GO at different concentrations (7.8–125 µg/mL) for 24 h. Statistical significance was observed between the highest concentration of GO and untreated cells ($p < 0.005$***, $p < 0.01$**).

to pGO in comparison to long pristine CNT after intraperitoneal (i.p.) injections. The inflammatory response was examined by the change in the protein levels and the number of polymorphonuclear leucocytes (PMN) after 24 h and 7 days. As shown in **Figure 5**, only the pristine long CNT caused a significant increase in PMN ($p < 0.005$) and protein levels after 24 h of exposure. Injections with graphite and the pGO showed a similar profile to naive (untreated) mice with low protein and PMN levels. After 7 days there was an overall decrease in protein and the total number of PMN cells, due to a change in the characteristics of the occurring inflammatory response, mainly manifested at later time points as granuloma formation (accumulation of macrophages and giant cells with a deposition of collagen) on the mesothelial membrane as previously described for this exposure model.[43] SEM images of the surface of the diaphragmatic mesothelial lining showed the collection of giant cells on the surface of mice treated with long pristine CNT but not with graphite or pGO material (**Figure 6**A&B). H&E histological sections of the membranes also confirmed that exposure to pristine, long CNT could lead to granuloma formation but not pGO (Figure 6C).

The exposure model used here to assess the toxicological profile of graphene oxide, has been developed and validated to determine the potential inflammatory and carcinogenic risk from exposure of fiber-shaped materials, namely asbestos and carbon nanotubes,[43,44] and it is not yet clear whether it is appropriate or suitably sensitive from exposure to two-dimensional, planar nanoscale graphene sheets. Schinwald et al.[26] recently used a very similar exposure model (based on intrapleural administrations) to assess the inflammatory risks from large and thick unmodified graphene '*nanoplatelets*', however no previous reports describe *in vivo* toxicity of GO using such exposure models. The pGO material in this study that was in the range between 100-500 nm in lateral dimensions were non-inflammogenic and did not cause granuloma formation after 7 days post-injection, in sharp contrast to long, pristine carbon nanotubes. This could be either due to efficient and complete phagocytosis of the small pGO sheets by resident peritoneal macrophages or their drainage from the peritoneal cavity to the cranial mediastinal lymph nodes. Such observations were in complete agreement with those by Schinwald et al.[26] who reported that the graphene '*nanoplatelets*' with projected area dimensions of 25 µm and thickness of 0.1µm (compared to 1–2 nm thickness of the pGO sample as shown in Figure S1) induced an inflammatory response and granuloma formation in the lung and pleural space. Moreover, such commercially available graphene '*nanoplatelet*' materials were not chemically or surface modified, therefore presumably hydrophobic and not very well dispersed, compared to pGO dispersions (Figure 1C) that were highly homogenous and colloidally stable. Duch et al.[45] have also previously highlighted the importance of adequate dispersibility to reduce any adverse reactions from direct exposure of the lungs to graphene. They reported that a stable aqueous dispersion of graphene in Pluronic F127 was non-fibrogenic to the lungs compared to aggregated graphene sheets following lung instillation.

Overall, these observations suggest further parameters to be considered as part of the nanomaterial toxicity paradigms used to assess safety risks. Graphene material dimensions (lateral and thickness) seem to be critical in leading an inflammatory reaction and granuloma formation to occur, despite the absence of the fibrous shape of the material. This suggests that the clearance kinetics of the nanomaterial from the site of exposure may be more important than previously thought. However, more issues remain unresolved in such interactions. The folding conformations of the graphene sheets *in vivo* are completely unknown presently, as well as the way in which graphene sheets interact with different cell types, membranes and anatomical barriers. Such investigations will need to be

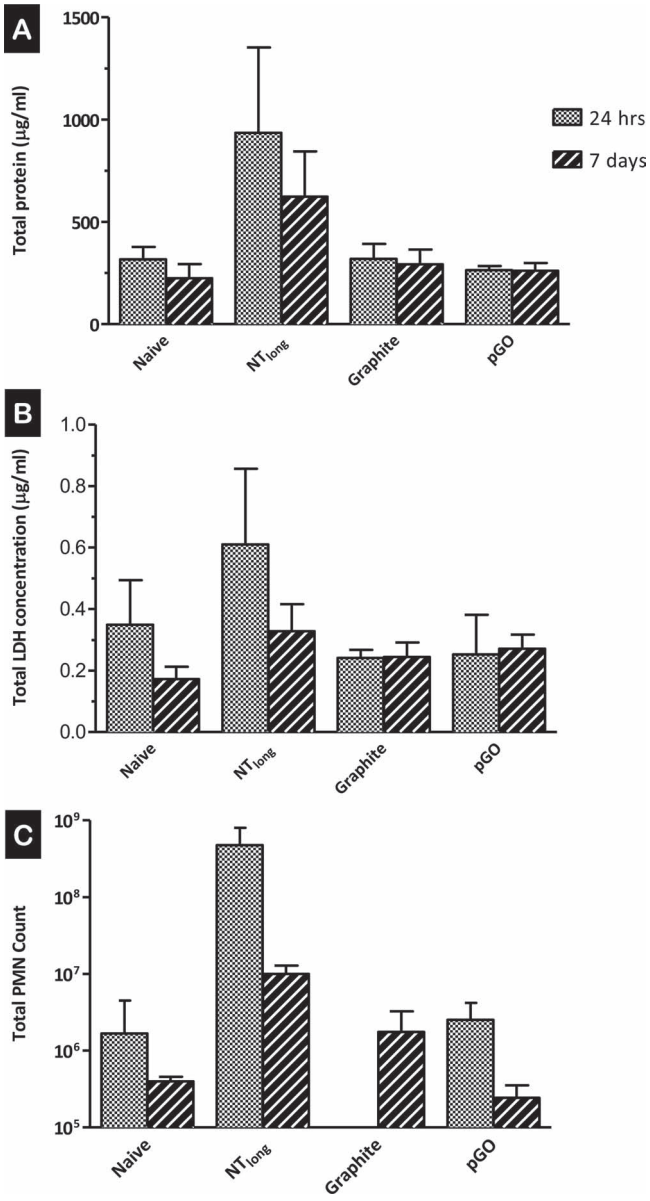

Figure 5. Inflammatory reaction in the peritoneal cavity 24 h and 7 days post-injection with GO. Female C57Bl/6 mice were intraperitoneally injected with 50 μg of vehicle control (0.5% BSA/saline), pGO dispersions and pristine MWNTs (NT_{long} Pristine) as positive control, the mice were killed and peritoneal cavity lavaged with saline. Inflammatory response was evaluated by: (A) total protein (protein exudation); (B) lactate dehydrogenase (LDH) release; and (C) the total polymorphonuclear leukocytes (PMN) after 24 h and 7 days. Data represent the mean of 4 animals +/− STDV.

carried out in order to confidently determine the safety profile of graphene materials.

3. Conclusion

In this study, we illustrated how the preparation of high purity, aqueous dispersibility and colloidal stability of single-layer GO sheets can be achieved using a simple modification of the conventional Hummers method. We report that pGO does not induce significant cytotoxic responses (for up to 100 μg/ml dose exposure) in vitro and no inflammation or granuloma formation (up to 50 μg/animal dose exposure) in vivo. A lot of further work is required to determine the mechanisms of interaction with cellular membranes and different cell types, and to identify the safety limitations that these interactions between single-layer GO sheets with living tissue may pose, in particular in view of recent studies[46] that report the presence of metallic impurities in chemically treated GO material and their reduced GO counterparts. On a broader context, while the vast majority of studies currently report use of impure GO, or centrifuged GO, that yield a mixed fraction of graphitic products, determination of their impact on interaction with living matter will remain difficult and unreliable.

4. Experimental Section

Preparation of graphene oxide (GO) with the conventional method: The oxidation of graphite was based on the Hummers method.[31] A mixture of 0.250g of Chinese fake graphite (Branwell) and 0.125g of sodium nitrate ($NaNO_3$) was placed in a conical glass fask. Temperature was kept around 0 °C by using an ice bath. A 5.75 ml of 96% sulphuric acid (H_2SO_4) were added and the mixture was stirred vigorously as the temperature should not exceed 20 °C. After obtaining a homogenized mixture, 0.750 g of potassium permanganate ($KMnO_4$) were added slowly. The temperature was monitored and did not exceed 10 °C. The mixture was removed from the ice bath after 10 min and temperature started to rise gradually. After 30 min the mixture started thickening and became a paste of dark brown/green color. 11.5 ml of deionized H_2O were added slowly while 18 °C stirring at the same time. Violent effervescence and rapid increase of temperature to 98 °C was observed. Temperature was monitored with a thermometer and was kept between 98–100 °C for another 30 min. The mixture was then further diluted with 35ml of deionised H_2O. 3% hydrogen peroxide (H_2O_2) aqueous solution was added gradually in small volumes until a sudden discoloration took place, indicating the reduction of the residual KMnO4, manganese dioxide (MnO_2) and manganese heptoxide (Mn_2O_7) to soluble manganese sulfate ($MnSO_4$) salts. The resulting suspension was then separated to two equal parts (A & B). Part A was centrifuged at 11000rpm and the supernatant was discarded. The remaining pellet was dried at 40 °C. The as- made-graphite oxide fakes were weighed and hydrated with deionized H_2O at a desired concentration. To exfoliate the graphene oxide fakes, sonication was performed in a water bath (Ultrasonic cleaner, VWR) for 15 min. The resulting dispersions of cGO were a mixture of graphite, non-dispersed graphite oxide, graphene oxide and by-products of the oxidation process. To remove any non-dispersed particles after the sonication step, we centrifuged the samples at 5000 rpm for 5 min. The supernatants (pGO) were carefully collected and the sediments were discarded.

Preparation of graphene oxide (GO) with the purified method: Part B from above was repeatedly washed by centrifugation at 9000rpm with warm water to remove the slightly soluble mellitic acid. The process was repeated until the discarded supernatant had a pH value equal to that of deionised H_2O (pH 6.9). As a result, the product was visibly separated in two portions of different color and consistency. The lower portion was made up of black particles and firmly adhered to the bottom of the tube. The upper portion was viscous, of yellow to brown color. It was readily dispersible in water and could be isolated by gently shaking the tube after adding 20ml of deionized H_2O. Upon suspending it in water, the color turned brown-orange. To determine the concentration of the orange-brown pGO from the modified Hummers method, a known volume was transferred into a glass vial and was dried at 40 °C for 24 hours. The residue was then placed in a vacuum desiccator for another 24 h in

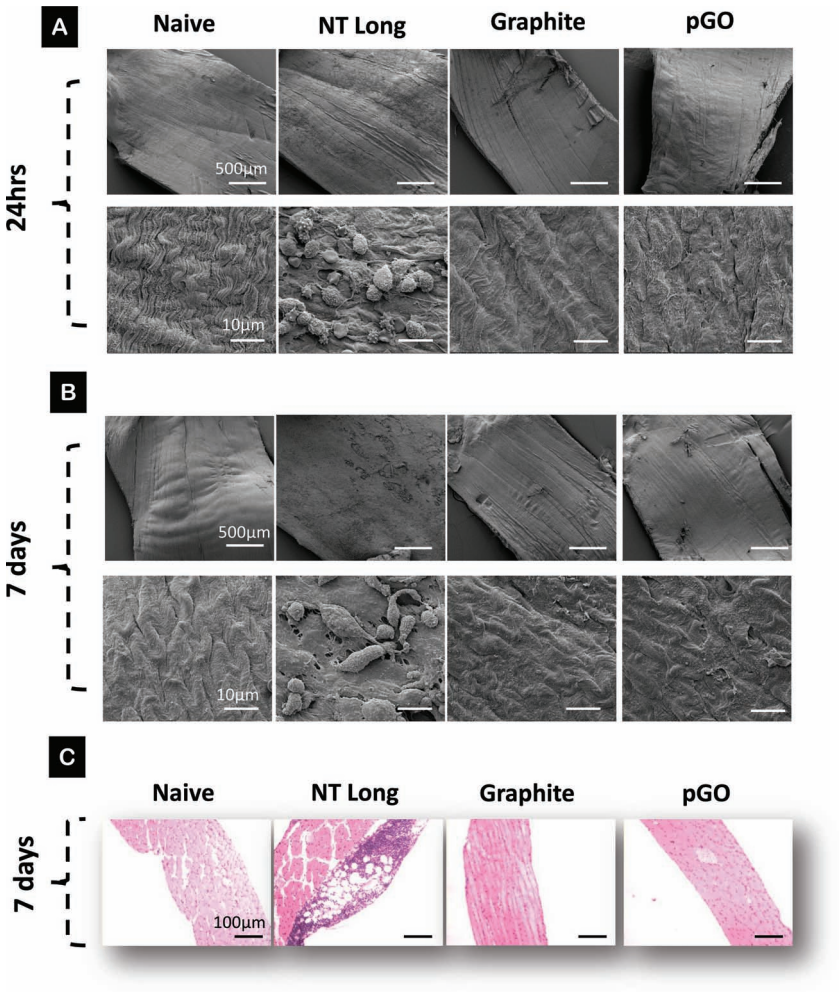

Figure 6. Granuloma formation on the diaphragm membrane after 7 days. Female C57Bl/6 mice were intraperitoneally injected with 50 µg of vehicle control (0.5% BSA/saline), pristine MWNTs (NT_{long} Pristine) and graphite and pure GO (pGO), the mice were killed after 24 h and 7 days and the diaphragms excised, fixed, and prepared for visualization. SEM images of the diaphragm surface (A–B), and the histology using H&E staining (C), highlights the presence of granulomatous inflammation with NT_{long}, but not with graphite and pGO. Low- and high-magnification of the SEM images are shown.

order to remove any remaining humidity. According to the weight of the dry product, the concentration of the original suspension was detected as 2.8mg/ml. It was then easy to dilute it to a desired concentration and sonicated for 15 min.

Transmission electron microscopy (TEM) of GO dispersions: A drop of the different GO dispersions was placed on a grid with a support film of Formvar/carbon, excess material was blotted off with a filter paper and the GO dispersions were examined under a FEI CM120 BioTwin Transmission Electron Microscope (Philips/FEI, USA) using a 80 KV electron beam current. Images were captured using an AMT Digital Camera.

Atomic force microscopy (AFM) of GO dispersions: A drop of the different GO dispersions was deposited on the surface of freshly cleaved mica (Agar Scientific, Essex, UK) and allowed to adsorb for 5 min. Unbound structures were removed by washing with 0.22 µm filtered deionized H_2O, then dried under a nitrogen stream. Imaging was carried out in Tapping Mode using a Multimode AFM, E-type scanner, Nanoscope IV controller, Nanoscope 5.12b control software (Veeco, Cambridge, UK) and a silicon tapping tip, made of crystallized silicon (NSG01, NTI-Europe, Apeldoorn, The Netherlands) of curvature radius of 10 nm. The tip was mounted on tapping-mode silicon cantilever with a typical resonant frequency of 150 kHz and a force constant of 5.5 N/m, to image 5 µm × 5 µm square areas of the mica surface, with a resolution of 512 × 512 pixels and a scan rate of 1 Hz.

Fourier-transform infrared (FTIR) spectroscopy: While the conventional cGO graphite oxide flakes were used as powder, the purified pGO suspensions were initially dried overnight at 40 °C in a glass vial. The dried graphene oxide films were scraped off the vial walls and where manually pressed into a pellet. Spectroscopy of the mid-infrared range was carried out on a PerkinElmer Spectrum 100 spectrophotometer and the transmittance results were analyzed with Spectrum software.

UV-Vis spectroscopy: The UV- Vis absorbance and spectra of cGO and pGO dispersions was determined using a Varian Cary 50 Bio spectrophotometer. The absorbance of the different GO dispersions as control was determined at a concentration of 50 µg/ml. Data was then analyzed with Cary Win UV software.

Raman spectroscopy: Raman spectra of the cGO and pGO samples were taken after depositing GO in water on to a pre-heated (50 °C) silicon substrate by drop casting. These samples consist of thin layer of overlapped individual GO flakes over millimetre area. Spectra were measured with a 50X objective at 514 nm excitation with a Renishaw micro-Raman spectrometer.

Culture of A549 monolayers: Epithelial lung carcinoma cells (A549; ATCC, CCL-185) were maintained and passaged in F12 Ham media supplemented with 10% FBS, 50 U/ml penicillin, 50 µg/ml streptomycin and 1% L-glutamine at 37 °C in 5% CO_2. Cells were passaged twice a week using trypsin-EDTA 0.05% when reaching 80% confluency.

Cellular interaction of GO with A549 cells: GO dispersions were used as sterile stock solutions at 1mg/ml (in 5% dextrose). A549 cells were seeded into 96-well plates (10,000 cells/well) and left to attach overnight before incubation with the GO dispersions. Cells were then incubated for 24 h with cGO and pGO (0-125 µg/ml) in complete media at 37 °C in a humidified atmosphere (5% CO_2). Monolayers were photographed using light microscopy after washing off the GO.

Cytotoxicity assessment of GO using modified LDH assay: LDH assay was subsequently modified to avoid any interference from GO similar to what was described with the CNT.[39] The LDH content was assessed in intact cells which survived the treatment, instead of detecting the amount of LDH released in the media upon GO induced-cell death. In brief, media was aspirated and cells were lysed with 10 µl of lysis buffer (0.9% Triton X100) mixed with 100 µl serum and phenol free media, for 45–60 min at 37 °C to obtain cell lysate which was then centrifuged at 16060xg for 5 min in order to pellet down the GO. Fifty microlitres of the supernatant of the cell lysate was mixed with 50 µl of LDH substrate mix in a new microtiter plate and incubated for 15 min at RT. Absorbance was read at 490 nm using a plate reader. The amount of LDH detected represented the number of cells which survived the treatment. The percentage cell survival was calculated using the following equation:

$$\text{Percentage Cell Survival} = \frac{A_{490\,nm}\ \text{of treated cells}}{A_{490\,nm}\ \text{of untreated cells}} \times 100$$

Toxicological effects of intraperitoneally injected pGO sample: Six- to eight-week-old C57BL6 mice were obtained from Harlan (Oxfordshire,

UK), allowed to acclimatise for 1 week and were kept in groups of 5 for the duration of the experiments and given food and water. All experiments were conducted with prior approval from the UK Home Office. Two groups of animals (n = 4–6) were intraperitoneally injected with 0.5 ml containing 50 μg of long, pristine multi-walled carbon nanotubes (NTlong), graphite and pGO in 0.5% BSA/saline (vehicle control; 0.5ml). One group of animals was scarified after 24 h and the other 7 days post-injection. The NTlong sample was a gift from Prof. K. Donaldson from the University of Edinburgh and was used as the positive control in this assay as previously published.[43]

Inflammatory reaction after injections of samples: 24 h and 7 days post-injection, mice were sacrificed by cervical dislocation and the peritoneum lavaged three times using 2 ml washes of sterile ice-cold PBS. The lavages were pooled together and placed on ice for the entire duration of the processing. The lavage fluid was then centrifuged at 1000 rpm for 5 minutes at 4 °C in a Hettich Universal 320R centrifuge (Hettich Zentrifuger, UK) and an aliquot of the supernatant was retained for total protein and LDH measurement. The remaining supernatant was discarded and the cell pellet re-suspended in 0.5 ml of 0.1% BSA/sterile saline solution and mixed with fluorescently labelled Ly-6C/G (Gr-1) antibody (Invitrogen, UK) that is used to differentiate polymorphonuclear leucocytes (PMN) from other cells. The GR-1 positive PMN leucocytes were quantified using flow cytometry. The assay with the Gr-1 antibody was performed according to the manufacturer's instructions. It is recommended that between 0.1 and 0.25 μg of antibody to be used per 1×10^6 cells in a 100 μl staining volume.

Total protein in the peritoneal lavage: Total protein concentration of the peritoneal lavage fluid was measured using the bicinchoninic acid (BCA) protein assay (Thermo Scientific Pierce, UK). The colorimetric assay was performed according to the manufacturer's instructions. Sample protein concentrations were established by comparison to a bovine serum albumin BSA standard curve (0–1000 μg/ml). The standard solutions and samples (10 μl) were loaded into 96-well plate. The reagent mixture was prepared by adding 1 part of reagent B to 50 parts of reagent A. After the colour change of the mixture (colourless to greenish), 200 μl of the mixture was added to each well. This assay is time dependent, so the samples were 37°C for 30 min before reading their absorbance at 562 nm using Victor Multilabel plate reader. The protein concentration of each sample was determined via extrapolation from the BSA standard curve.

The assessment of granuloma formation after 7 days post-injection: After 7 days, the abdominal wall was dissected free, exposing the peritoneal cavity via a midventral incision with lateral incisions extending to the veterebral column, which was then severed below the diaphragm. The diaphragm was then carefully dissected by cutting through the ribs and chest wall with care taken not to puncture the diaphragm as previously described by Poland et al.[42] The diaphragm was gently rinsed three times by emersion in ice-cold sterile PBS and placed overnight into:

- Methacarn fixative (60% methanol, 30% chloroform and 10% glacial acetic acid) for histological staining or
- 3% glutaraldehyde/0.1 M sodium cacodylate (pH 7.2) buffer for scanning electron microscopy (SEM) of the diaphragm surface.

After overnight incubation in fixative, the diaphragm was carefully excised from the surrounding ribs prior to further processing for either histological or SEM analysis.[43]

Histological examination diaphragm tissue: The diaphragm was then removed from the ribs and a similar section of the upper quadrant of the diaphragm was removed from each animal. This excised tissue was dehydrated through graded alcohol (ethanol) and imbedded on-edge in paraffin.[43] Four μm sections of the diaphragm were stained with hematoxylin and eosin stain by the Laboratory Diagnostic Service of the Royal Veterinary College (London, UK). Microscopic observation of tissues was carried out with Nikon Microphot-FXA microscope coupled with Infinity 2 digital camera.

Supporting Information

Supporting Information is available from the Wiley Online Library or from the author.

Acknowledgements

Part of the work described in this article was supported by the European Union FP7 ANTICARB program (HEALTH-2007-201587). H.A-B is a recipient of the postdoctoral Maplethorpe Fellowship from the University of London. We would like to acknowledge Professors Andre Geim and Kostya Novoselov for their guidance and advice at the early stages of this project and the provision of the graphite samples used in the preparation of graphene oxide. We also wish to acknowledge Mr. David McCarthy, UCL School of Pharmacy, for assistance with TEM and SEM photographs.

Received: May 18, 2012
Published online: October 4, 2012

[1] A. K. Geim, *Science.* **2009**, *324*, 1530.
[2] A. K. Geim, K. S. Novoselov, *Nature. Mater.* **2007**, *6*, 183.
[3] M. J. Allen, V. C. Tung, R. B. Kaner, *Chem. Rev.* **2009**, *110*, 132.
[4] C. N. R. Rao, A. K. Sood, K. S. Subrahmanyam, A. Govindaraj, *Angew.Chem. Int. Ed.* **2009**, *48*, 7552.
[5] S. Park, R. S. Ruoff, *Nat. Nanotechnol.* **2009**, *4*, 217.
[6] Y. Wang, Z. Li, J. Wang, J. Li, Y. Lin, *Trends Biotechnol.* **2011**, *29*, 205.
[7] C. Ge, J. Du, L. Zhao, L. Wang, Y. Liu, D. Li, Y. Yang, R. Zhou, Y. Zhao, Z. Chai, C. Chen, *Proc. Natl. Acad. Sci. USA.* **2011**, *108*, 16968.
[8] C.-H. Lu, H.-H. Yang, C.-L. Zhu, X. Chen, G.-N. Chen, *Angew.Chem. Int. Ed.* **2009**, *48*, 4785.
[9] H. Wang, Q. Zhang, X. Chu, T. Chen, J. Ge, R. Yu, *Angew. Chem. Int. Ed.* **2011**, *50*, 7065.
[10] L. Feng, Y. Chen, J. Ren, X. Qu, *Biomaterials.* **2011**, *32*, 2930.
[11] X. Sun, Z. Liu, K. Welsher, J. Robinson, A. Goodwin, S. Zaric, H. Dai, *Nano Res.* **2008**, *1*, 203.
[12] L. Feng, S. Zhang, Z. Liu, *Nanoscale.* **2011**, *3*, 1252.
[13] J. T. Robinson, S. M. Tabakman, Y. Liang, H. Wang, H. Sanchez Casalongue, D. Vinh, H. Dai, *J. Am. Chem. Soc.* **2011**, *133*, 6825.
[14] C. Peng, W. Hu, Y. Zhou, C. Fan, Q. Huang, *Small.* **2010**, *6*, 1686.
[15] H. Hong, Y. Zhang, J. W. Engle, T. R. Nayak, C. P. Theuer, R. J. Nickles, T. E. Barnhart, W. Cai, *Biomaterials.* **2012**, *33*, 4147.
[16] L. Zhang, J. Xia, Q. Zhao, L. Liu, Z. Zhang, *Small.* **2010**, *6*, 537.
[17] X. Yang, X. Zhang, Z. Liu, Y. Ma, Y. Huang, Y. Chen, *J. Phys. Chem. C.* **2008**, *112*, 17554.
[18] V. C. Sanchez, A. Jachak, R. H. Hurt, A. B. Kane, *Chem. Res. Toxicol.* **2012**, *25*, 15.
[19] K. Yang, S. Zhang, G. Zhang, X. Sun, S.-T. Lee, Z. Liu, *Nano Letters.* **2010**, *10*, 3318.
[20] Y. Chang, S.-T. Yang, J.-H. Liu, E. Dong, Y. Wang, A. Cao, Y. Liu, H. Wang, *Toxicol. Lett.* **2011**, *200*, 201.
[21] Y. Zhang, S. F. Ali, E. Dervishi, Y. Xu, Z. Li, D. Casciano, A. S. Biris, *ACS Nano.* **2010**, *4*, 3181.
[22] S. K. Singh, M. K. Singh, M. K. Nayak, S. Kumari, S. Shrivastava, J. J. A. Grácio, D. Dash, *ACS Nano.* **2011**, *5*, 4987.
[23] X. Zhang, J. Yin, C. Peng, W. Hu, Z. Zhu, W. Li, C. Fan, Q. Huang, *Carbon.* **2011**, *49*, 986.
[24] K. Yang, J. Wan, S. Zhang, Y. Zhang, S.-T. Lee, Z. Liu, *ACS Nano.* **2011**, *5*, 516.
[25] W. Hu, C. Peng, M. Lv, X. Li, Y. Zhang, N. Chen, C. Fan, Q. Huang, *ACS Nano.* **2011**, *5*, 3693.
[26] A. Schinwald, F. A. Murphy, A. Jones, W. MacNee, K. Donaldson, *ACS Nano.* **2011**, *6*, 736.
[27] L. Yan, Y. Wang, X. Xu, C. Zeng, J. Hou, M. Lin, J. Xu, F. Sun, X. Huang, L. Dai, F. Lu, Y. Liu, *Chem. Res. Toxicol.* **2012**, *25*1265.
[28] S. Agarwal, X. Zhou, F. Ye, Q. He, G. C. K. Chen, J. Soo, F. Boey, H. Zhang, P. Chen, *Langmuir.* **2010**, *26*, 2244.

[29] B. Fubini, M. Ghiazza, I. Fenoglio, *Nanotoxicology.* **2010**, *4*, 347.
[30] C. M. Sayes, D. B. Warheit, *Wiley. Interdiscip. Rev. Nanomed. Nanobiotechnol.* **2009**, *1*, 660.
[31] W. S. Hummers, R. E. Offeman, *J. Am. Chem. Soc.* **1958**, *80*, 1339.
[32] S. Niyogi, E. Bekyarova, M. E. Itkis, J. L. McWilliams, M. A. Hamon, R. C. Haddon, *J. Am. Chem. Soc.* **2006**, *128*, 7720.
[33] S. K. Singh, M. K. Singh, P. P. Kulkarni, V. K. Sonkar, J. J. A. Grácio, D. Dash, *ACS Nano.* **2012**, *6*, 2731.
[34] J. P. Rourke, P. A. Pandey, J. J. Moore, M. Bates, I. A. Kinloch, R. J. Young, N. R. Wilson, *Angew. Chem.* **2011**, *123*, 3231.
[35] D. A. Dikin, S. Stankovich, E. J. Zimney, R. D. Piner, G. H. B. Dommett, G. Evmenenko, S. T. Nguyen, R. S. Ruoff, *Nature.* **2007**, *448*, 457.
[36] D. C. Marcano, D. V. Kosynkin, J. M. Berlin, A. Sinitskii, Z. Sun, A. Slesarev, L. B. Alemany, W. Lu, J. M. Tour, *ACS Nano.* **2010**, *4*, 4806.
[37] Q. Mei, K. Zhang, G. Guan, B. Liu, S. Wang, Z. Zhang, *Chem. Commun.* **2010**, *46*, 7319.
[38] Z.-J. Fan, W. Kai, J. Yan, T. Wei, L.-J. Zhi, J. Feng, Y.-m. Ren, L.-P. Song, F. Wei, *ACS Nano.* **2010**, *5*, 191.
[39] H. Ali-Boucetta, K. T. Al-Jamal, H. K. Müller, S. Li, E. A. Porter, A. Eddaoudi, M. Prato, A. Bianco, K. Kostarelos, *Small.* **2011**, *7*, 3230.
[40] J. M. Worle-Knirsch, K. Pulskamp, H. F. Krug, *Nano Letters.* **2006**, *6*, 1261.
[41] H. Ali-Boucetta, K. T. Al-Jamal, K. Kostarelos, in *Biomedical Nanotechnology: Methods and Protocols, Methods in Molecular Biology*, Vol. *726* (Ed: S. J. Hurst, Springer Science **2011**.
[42] B. J. Hong, O. C. Compton, Z. An, I. Eryazici, S. T. Nguyen, *ACS Nano.* **2012**, *6*, 63.
[43] C. A. Poland, R. Duffin, I. Kinloch, A. Maynard, W. A. H. Wallace, A. Seaton, V. Stone, S. Brown, W. MacNee, K. Donaldson, *Nat. Nanotechnol.* **2008**, *3*, 423.
[44] H. Nagai, Y. Okazaki, S. H. Chew, N. Misawa, Y. Yamashita, S. Akatsuka, T. Ishihara, K. Yamashita, Y. Yoshikawa, H. Yasui, L. Jiang, H. Ohara, T. Takahashi, G. Ichihara, K. Kostarelos, Y. Miyata, H. Shinohara, S. Toyokuni, *Proc. Natl. Acad. Sci. USA.* **2011**, *108*, E1330.
[45] M. C. Duch, G. R. S. Budinger, Y. T. Liang, S. Soberanes, D. Urich, S. E. Chiarella, L. A. Campochiaro, A. Gonzalez, N. S. Chandel, M. C. Hersam, G. M. Mutlu, *Nano Letters.* **2011**, *11*, 5201.
[46] A. Ambrosi, C. K. Chua, B. Khezri, Z. Sofer, R. D. Webster, M. Pumera, *Proc. Natl. Acad. Sci. USA.* **2012**, *109*, 12899.